Importance of tip sensing for active control system of 30-m RIT primary mirror

Yichun Dai (戴懿纯)*, Zhong Liu (刘 忠), and Zhenyu Jin (金振宇)

Yunnan Astronomical Observatory, Chinese Academy of Sciences, Kunming 650011, China

**E-mail: daiyichun@ynao.ac.cn*

Received December 16, 2008

The active control of 30-m ring interferometric telescope (RIT) needs edge sensing and tip sensing when its primary mirror is composed by trapezoid-shaped segments, and the imaging performance of the RIT is determined by the accuracy of these two detecting approaches. Considering the detecting accuracy available in current segmented telescope active control systems, the effect of these detecting approaches on the surface error of the RIT primary mirror is calculated from the point of error propagation. The corresponding effect on imaging performance (modulation transfer functions (MTFs) and point spread functions (PSFs) at several typical wavelengths) of the RIT primary mirror is also simulated. The results show that tip sensing is very important for increasing the active control quality of the RIT primary mirror under the present techniques.

OCIS codes: 120.5050, 110.6770, 110.1080, 010.7350.

doi: 10.3788/COL20090709.0791.

The 30-m ring interferometric telescope (RIT)[1−3] (see http://rit.ynao.ac.cn) is a new-concept extremely large telescope (ELT) project. The primary mirror of the RIT is different from those of conventional ELTs[4,5], and it is a ring with 30-m outer diameter and the width of the ring is 1 m. Ninety trapezoid-shaped segments with the size of approximatly 1×1 (m) are expected to compose the ring primary mirror. The telescope looks like a Fizeau interferometer by appearance, while it has complete imaging ability. This is the reason why it is named RIT. The RIT has a colleting area equivalent to that of a 10-m-diameter telescope and a resolution of a 30-m-diameter telescope. Compared with a full-aperture telescope, the ring structure facilitates the RIT in its optical and structural design, and instrumental and focusing configuration. At the same time, the active control of the RIT's primary mirror is different from that of a full-aperture ELT for its typical structure. The active control for highly segmented primary mirror is widely used for large telescope with diameter larger than 8 m. The primary mirror is stabilized against perturbations due to gravity and thermal effects by actively positioning each segment. Segments are moved by actuators, while detecting of variations of segments is directly related to the segmented pattern of the primary mirror. Electromechanical edge sensors are sufficient for detecting task for a full-aperture telescope segmented by hexagonal sub-mirrors[6,7], but in the case of the RIT with trapezoid-shaped segments, some other techniques besides the electromechanical edge sensors are required to detect the tip variations of segments[8,9].

At present, the noise level of electromechanical edge sensors used for large segmented telescope is 1−5 nm[10,11], but this kind of edge sensors can only detect the relative displacements of adjacent segments, and the zero points of edge sensors are determined by other optical means. For instance, the Keck telescopes[7] use the diffraction patterns formed by subapertures at the center of each intersegment edges to determine the zero points of electromechanical edge sensors. The accuracy of this optical alignment is 20−30 nm[12,13]. The Gran Telescopio Canarias (GTC) telescope[14] and relative research[15] are ready to use a moveable interferometer to do optical alignment, and the accuracy can approach 5−7 nm in the laboratory[16,17]. Because electromechanical sensing and optical alignment are mutually independent, the edge error contributed by these two processes is about 5−31 nm (which is equal to the square root of the quadratic sum of the separate errors). Meanwhile, Shack-Hartmann (S-H) detection is a well developed technique to detect tip variation, and its sensing accuracy for tip variations of segments is 0.02−0.04 arcsec[18−20]. The above data are all root-mean-square (RMS) errors. Assuming that $P_{\rm tip}$ is tip sensing accuracy, and L is the baseline (the distance between the center and the edge of a segment), accordingly, $P_{\rm tip}L$ is the edge height accuracy corresponding to the tip sensing accuracy. For a 1-m segment, the edge height accuracy is 50−100 nm, corresponding to 0.02−0.04 arcsec of the tip sensing. So the accuracy level of tip sensing is lower than that of the present edge sensing.

The RIT primary mirror has 90 segments, as shown in Fig. 1. The piston (translation around the segment normal), tip (rotation around Y axis, see Fig. 2), and tilt (rotation around X axis, also see Fig. 2, each segment has its own coordinate system with different orientation from one to another), three out-of-plane degrees of freedom, of each segment are actively adjusted through three actuators on the back of the segment. The variations of the segmented surface are detected by S-H sensor and a set of electromechanical sensors which are mounted in pair on the edge of two neighboring segments. In the linear range of actuators and sensors, variations in sensor reading induced by variations in actuator length satisfy

$$\Delta\mathbf{y} = \mathbf{A}\Delta\mathbf{x} + \delta, \tag{1}$$

where the elements are all vectors or matrix. $\Delta\mathbf{y}$ and

$\Delta\mathbf{x}$ represent the variations in sensor reading and actuator length, respectively; δ is the desired sensor readings determined by optical alignment; $\mathbf{A}$ is the control matrix governing the active control system, and it is related to segmented pattern, segment geometry, type of sensors, and placement of actuators and sensors. In the case of RIT, $\mathbf{A}$ is also related to the detecting ability (detecting accuracy) of edge sensors and S-H sensor because these two kinds of sensors are involved in the RIT's active control loop. The detailed construction of RIT's control matrix can be found in Ref. [8]. Figure 2 shows the segment geometry, placement of actuators and electromechanical edge sensors, and other related parameters used for matrix construction. The surface error of the RIT primary mirror induced by active control system, which is nearly equal to the RMS actuator length error (actuator noise is ignored here), depends on the accuracy of edge sensing and tip sensing when the parameters given in Fig. 2 are fixed. The desired changes in the actuator length can be acquired from the sensor information and matrix $\mathbf{A}^{\#}$ which is the pseudo-inverse matrix of the control matrix $\mathbf{A}$:

$$\Delta\mathbf{x} = \mathbf{A}^{\#}\left(\Delta\mathbf{y} - \delta\right). \tag{2}$$

The detecting errors in sensors will affect the final actuator length through $\mathbf{A}^{\#}$, and the overall error multiplier is the evaluating index for this error propagation of sensors[21,22]:

$$N = \left(\sum_{j=1}^{n_{\mathrm{act}}} w_j^{-2}/n_{\mathrm{act}}\right)^{1/2}, \tag{3}$$

where N is the overall error multiplier, w_j^{-1} is the singular value[23] of $\mathbf{A}^{\#}$, and n_{act} is the mode number of primary mirror deformation that can be detected by sensors in the active control loop[22]. The RMS surface error of the primary mirror is

$$\Delta_{\mathrm{rms}} = N\Phi, \tag{4}$$

where Φ is the RMS accuracy of sensors.

Supposing that the accuracy of edge sensing is 10 nm, the overall error multiplier varying with the accuracy of tip sensing is illustrated in Fig. 3. It is easy to see that the overall error multiplier is deeply influenced by the accuracy of tip sensing. The multiplier decreases almost linearly with the increase of tip sensing accuracy, consequently, the surface error of primary mirror decreases linearly from Eq. (4). With the combined accuracies of edge sensing and tip sensing to (10 nm, 0.004 arcsec) and (10 nm, 0.04 arcsec), respectively, the modulation transfer functions (MTFs) of the RIT primary mirror at the wavelengths of 550, 1500, and 2500 nm are presented in Fig. 4. It is evident that increasing the accuracy of tip sensing can improve the MTF of the RIT primary mirror at the wavelengths of 1500 and 2500 nm, and the RIT primary mirror can realize diffraction-limited imaging at the above wavelengths if the accuracy of tip sensing achieves 0.004 arcsec. This tip sensing accuracy is just the theoretical value. In this case, a sensor with higher precision is needed instead of the traditional S-H sensor.

In the meantime, with the accuracy of tip sensing at a level of 0.02 arcsec (it is 50 nm when converted to edge height), and in the accuracy range of edge sensing of 5−30 nm, the overall error multiplier variation with the accuracy of edge sensing is given in Fig. 5. It is shown that when the accuracy of tip sensing is relatively low, increasing the accuracy of edge sensing can do little help to decrease the overall error multiplier. In this instance, the overall error multiplier and corresponding surface error of the primary mirror depend mainly on the accuracy of tip sensing. Figure 6 presents the MTFs of the RIT primary mirror at the wavelengths of 550, 1500, and 2500 nm with the combined accuracies of (5 nm, 0.02 arcsec) and (30 nm, 0.02 arcsec), respectively. It is shown from the figures that by increasing the accuracy of edge sensing,

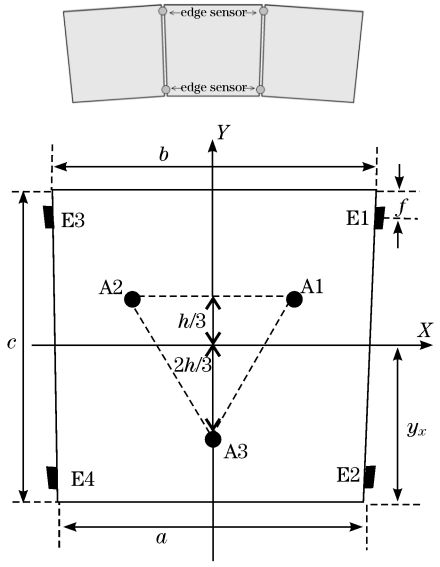

Fig. 2. Distribution of 3 actuators (A1−A3) and 4 edge sensors (E1−E4) on a trapezoidal segment. X and Y represent two in-plane axes of the segment; a=975 mm, b=1045 mm, c=1000 mm, h=450 mm, y_x=506 mm, f=86 mm.

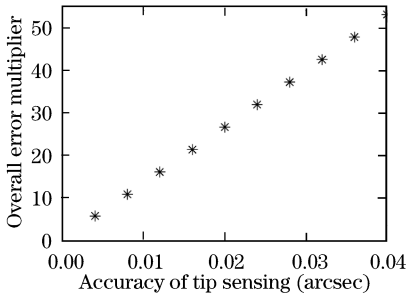

Fig. 3. Overall error multiplier variation with the RMS accuracy of tip sensing.

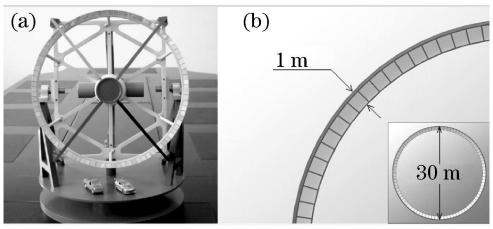

Fig. 1. (a) Model of the 30-m RIT and (b) size of its trapezoidal segments.

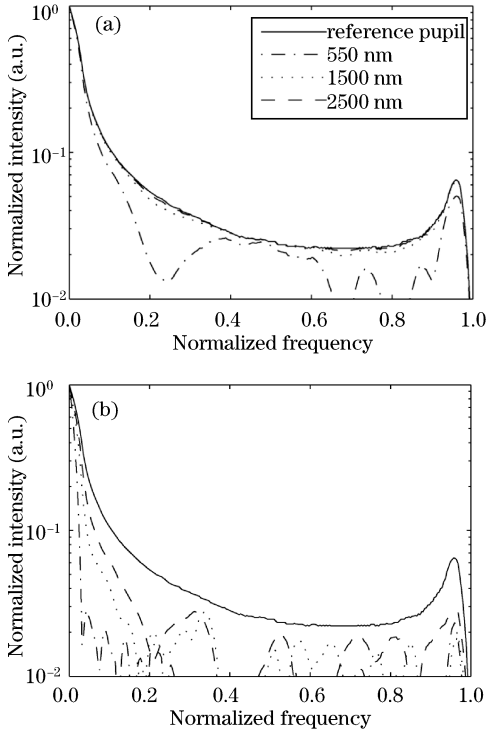

Fig. 4. MTFs of the RIT primary mirror with edge sensing accuracy of 10 nm and tip sensing accuracy of (a) 0.004 arcsec and (b) 0.04 arcsec.

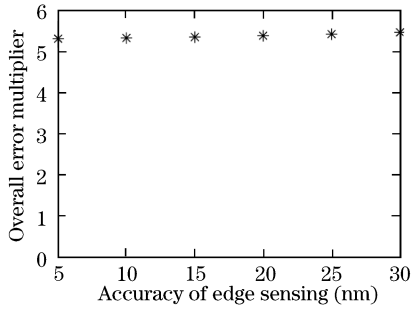

Fig. 5. Overall error multiplier variation with the RMS accuracy of edge sensing.

the MTF characteristics of the RIT could not be improved effectively. Moreover, the perfect point spread function (PSF) of the 30-m RIT primary mirror is shown in Fig. 7. The corresponding PSF with combined accuracy of (5 nm, 0.02 arcsec) at the wavelength of 1500 nm is presented in Fig. 8(a), and the PSF with combined accuracy of (10 nm, 0.004 arcsec) at the same wavelength is given in Fig. 8(b).

In fact, since tip sensing and edge sensing are mutually independent processes in the RIT primary active control loop, the overall error multiplier N can be expressed as

$$N = \sqrt{N_{\text{edge}}^2 + N_{\text{tip}}^2}, \tag{5}$$

where N_{edge} is the error multiplier only contributed by edge sensing with perfect tip sensing (without any error in tip sensing), and N_{tip} is the error multiplier only contributed by tip sensing with perfect edge sensing. In the RIT control loop, $N_{\text{edge}} = 2.1840$, and $N_{\text{tip}} = 5.3220$, thus the overall error multiplier contributed by both edge

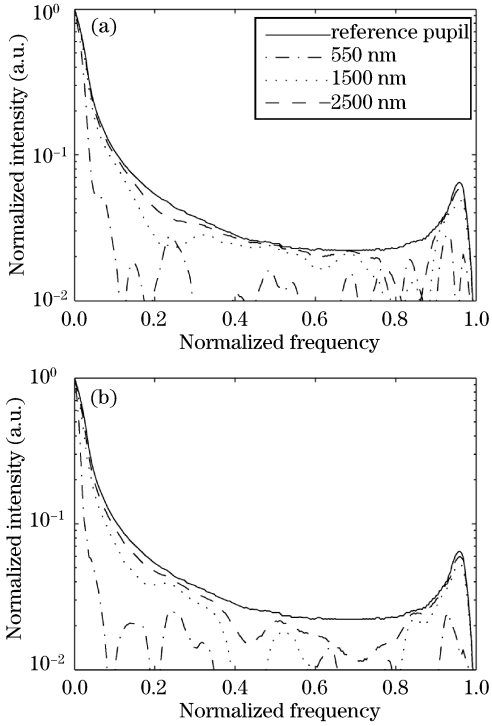

Fig. 6. MTFs of the RIT primary mirror with tip sensing accuracy of 0.02 arcsec and edge sensing accuracy of (a) 5 nm and (b) 30 nm.

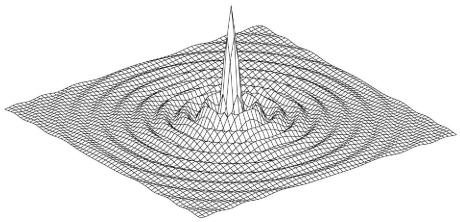

Fig. 7. Perfect PSF of the 30-m RIT primary mirror.

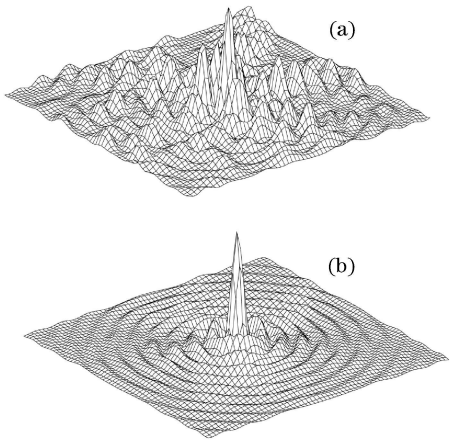

Fig. 8. PSFs of RIT primary mirror at the wavelength of 1500 nm with (a) edge sensing accuracy of 5 nm and tip sensing accuracy of 0.02 arcsec; (b) edge sensing accuracy of 10 nm and tip sensing accuracy of 0.004 arcsec.

sensing and tip sensing is 5.7527. It means that the tip sensing contributes more to the overall error multiplier. If the accuracy ratio of edge sensing to tip sensing is de-

fined as ρ, then Eq. (5) can be modified to

$$N = \sqrt{\rho^2 N_{\text{edge}}^2 + N_{\text{tip}}^2}. \quad (6)$$

Here, the edge sensing accuracy is higher than tip sensing accuracy when $0 \leq \rho \leq 1$. It is obvious that the overall error multiplier is mainly determined by tip sensing in the case of $\rho N_{\text{edge}} \ll N_{\text{tip}}$. Therefore, theoretically, the tip sensing accuracy also dominates the overall error multiplier and the final surface error.

From the above discussions, it can be concluded that since two detecting techniques are adopted in the RIT primary mirror active control loop, the edge sensing accuracy is higher than the tip sensing accuracy, and increasing the tip sensing accuracy will be helpful to reduce the surface error and improve imaging performance. So high accuracy of tip sensing is crucial for the active control of the RIT primary mirror.

This work was supported by the National Natural Science Foundation of China (Nos. 10573035, 10533040) and the National "973" Program of China (No. 2006CB806300).

References

1. Z. Liu, Z. Jin, Y. Li, J. Lin, and H. Tan, Proc. SPIE **6267,** 62672L (2006).
2. Z. Liu and X. Cui, Proc. SPIE **6986,** 698606 (2008).
3. J. R. P. Angel, A. Y. S. Cheng, and N. J. Woolf, Nature **322,** 341 (1986).
4. "Thirty meter telescope construction proposal" (Sep. 12, 2007) available online at http://www.tmt.org/news/TMT-Construction Proposal-Public.pdf.
5. R. Gilmozzi and J. Spyromilio, "The European extremely large telescope (E-ELT)" available online at http://www.eso.org/sci/publications/messenger/archive/no.127-mar07/gilmozzi.pdf.
6. T. S. Mast and J. E. Nelson, Appl. Opt. **21,** 2631 (1982).
7. R. C. Jared, A. A. Arthur, S. Andreae, A. Biocca, R. W. Cohen, J. M. Fuertes, J. Franck, G. Gabor, J. Llacer, T. Mast, J. Meng, T. Merrick, R. Minor, J. Nelson, M. Orayani, P. Salz, B. Schaefer, and C. Witebsky, Proc. SPIE **1236,** 996 (1990).
8. Y. Dai, "Research on active control of primary mirror of 30m ring interferometric telescope" PhD Thesis (Yunnan Astronomical Observatory, Kunming, 2008).
9. Y. Dai, Z. Liu, Z. Jin, J. Xu, and J. Lin, Appl. Opt. **48,** 664 (2009).
10. D. G. MacMartin and G. Chanan, Proc. SPIE **4840,** 69 (2003).
11. R. H. Minor, A. A. Arthur, G. Gabor, H. G. Jackson, R. C. Jared, T. S. Mast, and B. A. Schaefer, Proc. SPIE **1236,** 1009 (1990).
12. G. Chanan, M. Troy, F. Dekens, S. Michaels, J. Nelson, T. Mast, and D. Kirkman, Appl. Opt. **37,** 140 (1998).
13. G. Chanan, C. Ohara, and M. Troy, Appl. Opt. **39,** 4706 (2000).
14. P. Alvarez, J. M. Rodriguez-Espinosa, and F. R. Kabana, Proc. SPIE **4004,** 26 (2000).
15. H. Song, H. Li, H. Xian, R. Yang, J. Huang, and W. Jiang, Acta Opt. Sin. (in Chinese) **28,** 1523 (2008).
16. A. Pintó, F. Laguarta, R. Artigas, and C. Cadevall, J. Opt. A **4,** S369 (2002).
17. C. Pizarro, J. Arasa, F. Laguarta, N. Tomàs, and A. Pintó, Appl. Opt. **41,** 4562 (2002).
18. M. Troy, G. Chanan, E. Sirko, and E. Leffert, Proc. SPIE **3352,** 307 (1998).
19. G. Chanan, J. Nelson, T. Mast, P. Wizinowich, and B. Schaefer, Proc. SPIE **2198,** 1139 (1994).
20. X. Hu, X. Yu, and D. Zhao, Acta Opt. Sin. (in Chinese) **27,** 1414 (2007).
21. G. Chanan, D. G. MacMartin, J. Nelson, and T. Mast, Appl. Opt. **43,** 1223 (2004).
22. D. G. MacMartin and G. Chanan, Appl. Opt. **43,** 608 (2004).
23. J. Luo, *Introduction to Matrix Analysis* (in Chinese) (South China University of Technology Press, Guangzhou, 2001).